CrystEngComm

ROYAL SOCIETY OF CHEMISTRY

PAPER

View Article Online
View Journal | View Issue

Cite this: *CrystEngComm*, 2024, **26**, 6707

A family of luminescent heterometallic coordination polymers based on lanthanide(III) ions and 6-methyl-2-oxonicotinate: near-infrared/visible emitters and colour fine-tuning†

Laura Razquin-Bobillo, [a] Jose Angel García,[b] Ricardo Hernández,[a] Antonio Rodríguez-Diéguez [c] and Javier Cepeda *[a]

The work presented herein reports on the synthesis, structural and physicochemical characterization and luminescence properties of a family of isostructural coordination polymers (CPs) with a general formula $\{[Ln(6m2onic)_4Na(H_2O)_3]\cdot 8H_2O\}_n$ (where Ln(III) = Nd ($\mathbf{1}_{Nd}$), Sm ($\mathbf{2}_{Sm}$), Dy ($\mathbf{3}_{Dy}$), Er ($\mathbf{4}_{Er}$), Tm ($\mathbf{5}_{Tm}$), Yb ($\mathbf{6}_{Yb}$) and $Dy_{0.77}Eu_{0.12}Y_{0.11}$ for the multi-metal compound ($\mathbf{7}_{DyEuY}$) and 6m2onic = 6-methyl-2-oxonicotinate). The crystal structures consist of one-dimensional heterometallic arrays where octacoordinated lanthanide and hexacoordinated sodium centres are sequentially linked and which are held together into a 3D architecture by an extensive hydrogen bonding network formed by the crystallisation water molecules. Photoluminescence measurements in the solid state at variable temperature reveal good properties based on the capacity of the 6m2onic ligand to provide ligand-centred excitation, as suggested by time-dependent density functional theory (TDDFT), and promote efficient energy transfers to the lanthanide(III) ions, to eventually present intense emissions in both the visible and near-infrared (NIR) regions. On the one hand, compound $\mathbf{4}_{Er}$ displays characteristic lanthanide-centred bands in the NIR region even at room temperature, meaning that the framework is able to isolate the excitons from the vibrational quenching component. On the other hand, regarding the compounds emitting in the visible region, the almost white light emitted by compound $\mathbf{3}_{Dy}$ with a quantum yield (QY) of 6.2% should be noted. Both a purer white emission and an improved QY (up to 15.8%) may be achieved by means of a doping strategy of europium and yttrium ions into the Dy counterpart. Finally, taking advantage of white light emitted by compound $\mathbf{3}_{Dy}$, the chemical and optical stabilities in water have been confirmed by the photophysical study performed in solution.

Received 2nd September 2024,
Accepted 25th October 2024

DOI: 10.1039/d4ce00881b

rsc.li/crystengcomm

Introduction

The simultaneous occurrence of various physical properties in a crystalline material has made coordination polymers (CPs) very attractive to synthetic chemists designing functional materials given their applicability.[1,2] In fact, their modular architecture based on self-assembled metal ions and ligands can be grown by a previous design in which adequate components are selected, which permits predefining the properties of the material.[1,3–5] In particular, CPs have been studied in depth for their interesting characteristics in different fields such as magnetism,[6] luminescence,[7,8] catalysis,[9] biomedicine[10] and optoelectronics.[11] Moreover, those compounds showing permanent porosity (pores available after the removal of solvent molecules or other molecules occupying them), termed as metal–organic frameworks (MOFs), are acknowledged for their excellent performance in gas adsorption and separation,[12] sensory activity,[13] drug release,[14] heterogeneous catalysis,[15] and so on. With respect to metal ions, transition metal ions have been traditionally more used, mainly those of the first series, given their availability and well-defined coordination geometries, which helps in the aforementioned rational design. However, in spite of the more flexible coordination geometries shown derived from their higher coordination indices, lanthanide(III) (Ln) ions have been also successfully employed to yield CPs due to their unique magnetic and

[a] *Departamento de Química Aplicada, Facultad de Química, Universidad del País Vasco (UPV/EHU), 20018 Donostia-San Sebastián, Spain. E-mail: javier.cepeda@ehu.es*
[b] *Departamento de Física, Facultad de Ciencia y Tecnología, Universidad del País Vasco (UPV/EHU), 48940, Leioa, Spain*
[c] *Departamento de Química Inorgánica, Facultad de Ciencias, Universidad de Granada, 18071 Granada, Spain*

† Electronic supplementary information (ESI) available. CCDC 2378019–2378021. For ESI and crystallographic data in CIF or other electronic format see DOI: https://doi.org/10.1039/d4ce00881b

luminescence properties.[16–18] With special regard to luminescent Ln-based CPs, the research encompasses the preparation of compounds focusing on enhancing their emission capacity, to develop materials as phosphors not only in solid state lighting but also in bioimaging, and/or providing variable emission in response to the interaction of the luminescent material with a target molecule to perform as a sensor device.[19]

In the search and development of novel CPs with enhanced PL, the use of Ln ions as metal centres is particularly beneficial because their emission, based on the intrinsic f–f transitions, may extend along the UV-vis–IR regions.[20,21] The major drawback comes from the fact that these ions possess poor absorption capacity because f–f transitions are not allowed by Laporte's rule and thus generate narrow, low-intense absorption bands.[22,23] However, this problem can be solved by resorting to the well-known antenna effect, by which the ligand's absorption energy is transferred to the excited states of Ln to provide more brilliant emissions than those derived from intraionic f–f excitations.[7,8] In this sense, although most of the Ln(III) ions are potentially luminescent, they do not emit with the same intensity. In fact, the latter depends on the ease with which the emitting excited states are populated and on the accessibility of non-radiative pathways present.[24,25] For instance, the smaller the energy gap existing between the lowest energy excited level of the Ln(III) ion and the unfolded terms by the ground state's spin–orbit coupling (SOC), the more probable the non-radiative deactivation occurring through molecular vibrations in the ligand.[7]

On another level, the ligand field has little effect on the SOC levels of Ln ions; therefore, the emission bands appear at practically the same energy in all their complexes. This is precisely one of the great advantages of Ln ions, since their luminescence offers high colour purity, some of them, in turn, tune fundamental colours.[26,27] As a consequence, it can be said that these ions are excellent candidates for preparing luminescent compounds with multicolour emission due to their large Stokes shift and their long-lived and efficient emitted signal.[18] Depending on the type and relative concentration of different Lns, provided that they are compatible at the same metal site in the framework, the luminescence colour may be varied by mixing various Lns, or even using non-luminescent metal ions such as non-lanthanide yttrium(III), main group or group 12 metal ions which boost ligand centred luminescence. In this regard, although combining the latter ions with Lns in the synthesis may lead to heterometallic CPs with excellent properties related to magnetism and optics,[28–31] these sorts of compounds have been reported much scarcely in comparison with Ln-based CPs.[32] Among them, Ln–Na compounds are quite often achieved due to the passive use of Na^+ ions in the synthesis, especially by adding them as NaOH in order to deprotonate the ligand molecule and increase its solubility.[33] Leaving aside the benefits that the occurrence of these alkali ions in CPs could bring owing to their vital role played in many relevant biochemical processes, they may strongly modulate the structure, for instance, discriminating between chiral and achiral CPs.[33] Coming back to luminescence properties, the presence of Na^+ ions intercalated in the structure may also isolate Ln centres from each other, thus preventing the well-known quenching by luminophore concentration[34,35] and improving the emitted signal. Moreover, the appropriate combination of chromophores may allow fine-tuning of white light emission, a rare and very desired light in luminescent materials,[36] according to three main approaches involving mono-, di- or trichromatic emitters that combine one, two or three fundamental colours, respectively.[37] Moreover, among the various approaches to provide white light, the mixture of Lns can be optimized to increase the quantum yield (QY) considering the sensitization of the ligand by each of the monochromatic emitters.

Another point to consider about compounds with high luminescence performance is the thermal and chemical stabilities both in solid and aqueous states, which are advantageous for various applications such as chemical sensors, luminescent probes, OLEDs, laser systems and so on.[38–42] However, the combination of the above-mentioned stabilities is not frequently achieved in metal–organic systems, especially in the case of water solubility. While discrete complexes can benefit from higher capacity to dissolve in water keeping the coordination bonds unaltered,[43] CPs benefit from higher metal-to-ligand connectivity that is usually translated into higher thermal stability, whereas they present low solubility, particularly in water.[44]

Continuing with our quest for novel materials showing enhanced PL properties, and based on the previous ideas, we report herein on five isostructural 1D CPs formed from Ln(III) and Na ions and 6-methyl-2oxonicotinate (6m2onic) ligands, named as $\mathbf{1_{Nd}}$, $\mathbf{2_{Sm}}$, $\mathbf{3_{Dy}}$, $\mathbf{4_{Er}}$, $\mathbf{5_{Tm}}$ and $\mathbf{6_{Yb}}$. These compounds, isostructural to those behaving as single-molecule magnets,[45] present good luminescence properties due to the great capacity of the 6m2onic ligand to transfer the absorbed energy to the Ln(III) centres, generating metal-centred intense emissions in both visible and NIR regions with significantly good quantum yields (QYs). In addition to a detailed study of their performance in the solid state, involving experimental measurements and computational calculations to unravel the PL mechanism, compound $\mathbf{3_{Dy}}$ also proves to keep adequate emission in water solution with a white coloured emission. Taking advantage of this fact, the improvement of the quantum yield of the Dy-based compound and the enhancement of the white light emission by metal doping with different Ln ions have been studied, rendering single crystals of the multi-metal CP with a $Dy_{0.77}Eu_{0.12}Y_{0.11}$ proportion (estimated from the X-ray fluorescence (XRF) technique, see Table S3 in the ESI†) that presents a higher value of QY of 15.8% and pure white light emission.

Results and discussion

Structural description of {[Ln(6m2onic)$_2$(μ-6m2onic)$_2$Na(H$_2$O)$_3$]·8H$_2$O}$_n$ [where Ln(III) = Nd ($\mathbf{1_{Nd}}$), Sm ($\mathbf{2_{Sm}}$), Dy ($\mathbf{3_{Dy}}$), Er ($\mathbf{4_{Er}}$), Tm ($\mathbf{5_{Tm}}$) and Yb ($\mathbf{6_{Yb}}$)]

The title compounds are isostructural and pertain to a family of Ln-based CPs,[45] so only a brief structural description is provided here for compound $\mathbf{1_{Nd}}$. Their structure, crystallizing in the *Pbca* space group, is built from one-dimensional Ln/Na metal–organic chains that are further linked to one another into a weak crystal architecture formed by a large hydrogen bonding network of lattice water molecules (Fig. 1).

The asymmetric unit contains a Nd1 atom, one Na2 atom, four crystallographically independent 6m2onic ligand (the prototropic tautomers of 2h6mnic that favour the coordination to metal ions, see our previous computational study on the ligand prototropy)[46] copies (labelled A, B, C and D), three water molecules coordinated to the Na2 atom and eight crystallisation water molecules. The Nd1 atom presents an octacoordinated shell formed by eight oxygen atoms pertaining to four chelating ligands, which resembles a square antiprism in view of the low distortion parameter calculated by continuous shape measures (CShMs, S_{SAPR} = 0.524). The second centre (Na2), instead, presents a distorted NaO_6 octahedron (see Table S1†).[47] Both centres contain habitual coordination bond distances falling in the range of other related CPs (Table 1).[48,49] The four 6m2onic ligands show three distinct coordination patterns: i) ligands A and B present the κ^2-O,O′ mode by which six-membered chelating rings are established; ii) the C ligand, in addition to the latter ring, forms a second four-membered chelating ring with the Na2 atom according to the μ-κ^2-O,O′:κ^2-O′,O″ mode; iii) ligand D presents the μ-κ^2-O,O′:κ-O′ mode to extend the polymerization along the chain by a monodentate Na–O bond. It should be noted that C and D ligands bridge Nd1 and Na2 centres with each other at *ca.* 5.0 and 5.2 Å, respectively, giving rise to the mentioned 1D arrays (see Fig. 1).

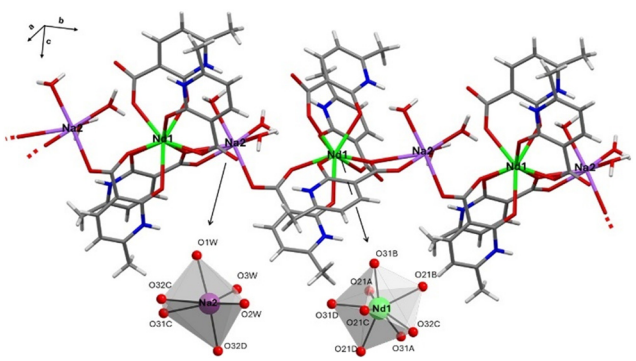

Fig. 1 View of a 1D array of compound $\mathbf{1_{Nd}}$. Coordination polyhedra are shown in detail with the corresponding numbering scheme. Colour codes: carbon (grey), hydrogen (white), nitrogen (blue), oxygen (red), neodymium (green) and sodium (purple).

The three-dimensional packing of the compound (see Fig. 2) is built by a large hydrogen-bonding network tailored by the crystallisation and coordination water molecules, which connects the metal–organic chains to one another. As a consequence, Ln ions are very far away in the framework, with the closest distances among Nd(III) ions pertaining to adjacent chains being *ca.* 9.41 Å (Fig. S13†).

PL properties of visible emitters ($\mathbf{2_{Sm}}$, $\mathbf{3_{Dy}}$ and $\mathbf{5_{Tm}}$) in the solid state

Lanthanide-based emissions in crystalline materials, such as CPs, are known to be useful for developing solid-state photodevices[50,51] given their intense emissions in the visible spectra or in the NIR region.[8,52] Therefore, photoluminescence measurements were performed on polycrystalline samples of all compounds to study their properties. To start with, we first inspected the PL of the visible emitters (Table 2). The sample of $\mathbf{2_{Sm}}$ was excited under laser irradiation (λ_{ex} = 325 nm) at RT to collect the corresponding emission spectrum (Fig. 3).

This spectrum is characterized for a first main band corresponding to the ligand emission peaking at 390 nm. In addition to this band, other narrow bands at λ_{em} = 565, 606, 652 and 714 nm are observed, which are attributed to the Ln-centred $^6H_J \leftarrow {}^4G_{5/2}$ transitions (J being 5/2, 7/2, 9/2 and 11/2).[8] In fact, when the excitation spectrum is recorded by monitoring the λ_{em} = 606 nm emission, an intense and broad band attributed to the ligand is observed followed by a set of narrow bands corresponding to transitions in the 4f subshell (Fig. S17†). It is remarkable that the intensity of these bands is significantly less intense compared to the ligand band (showing a main band centred at 355 nm accompanied by a shoulder at 305 nm, in agreement with the absorption bands observed by diffuse reflectance, see Fig. S14 and S16†), suggesting that the ligand exerts a good antenna effect. In contrast, when the sample temperature is lowered to 15 K, the Sm-centred emission lines are comparatively stronger, as expected for the enhancement of the antenna effect with decreasing temperature.

The excitation of compound $\mathbf{3_{Dy}}$ under UV laser light (λ_{ex} = 325 nm) gives an emission spectrum containing, apart from a very weak band covering the 360–450 nm range, the characteristic narrow bands ascribed to the Dy-centred transitions (Fig. 3). In particular, three single narrow bands are observed at 483, 578 and 667 nm which are assigned to $^6H_J \leftarrow {}^4F_{9/2}$ transitions (where J = 15/2, 13/2 and 11/2). The white colour emitted by this dysprosium-based compound (0.34, 0.38) should be noted, which is not very common in luminescent materials and usually requires Ln doping to adjust the white emission. In recent years, this strategy has been largely employed to prepare white light emitting materials with high efficiency.[36] Monitoring the main emission line, the excitation spectrum exhibits a wide band centred at 356 nm, which corresponds to ligand-centred excitation. The spectrum does not contain stronger narrow

Table 1 Selected bond lengths for compound $\mathbf{1_{Nd}}$ (Å)[a]

Coordination sphere of the Nd1 atom			
Nd1–O21A	2.467(1)	Nd1–O31A	2.399(1)
Nd1–O21B	2.475(1)	Nd1–O31B	2.471(1)
Nd1–O21C	2.405(1)	Nd1–O31D	2.382(1)
Nd1–O21D	2.440(1)	Nd1–O32C	2.413(4)
Coordination sphere of the Na2 atom			
Na2–O31C	2.336(1)	Na2–O1W	2.453(1)
Na2–O32C	2.376(1)	Na2–O2W	2.390(1)
Na2–O32D(i)	2.376(1)	Na2–O3W	2.319(2)

[a] Symmetries: (i) $x - 1/2, y, -z + 1/2$.

bands attributed to the intraionic f–f transitions (well distinguished at low temperature in the 380–400 nm region, see Fig. S20†), which means that the ligand exerts a good antenna effect. Cooling down the sample to 15 K brings an increase of the emission intensity (see the ESI†) that, in the present case, is not only motivated by the decrease of the vibrational quenching but also by the blue-shift occurring at low temperature for the main ligand-centred band, in such a way that the intensity is higher at λ_{ex} = 325 nm (see Fig. S20†). Under a monochromatic laser beam (λ_{ex} = 325 nm), the emission spectrum of $\mathbf{5_{Tm}}$ displays a broad band corresponding to the ligand emission and, in addition, a multiplet centred at 482 nm which is assigned to the $^3H_6 \leftarrow {}^1G_4$ transition. It is worth noting that, although metal–organic Tm-based emitters have not been largely discussed so far, the mentioned emission resembles those found for other complexes in the bibliography.[53] Regarding the excitation spectra recorded at the ligand- (λ_{em} = 398 nm) and Tm-centred (λ_{em} = 482 nm) emissions, both of them show a main wide band peaking at *ca.* 360 nm, in good agreement with previous compounds, although some narrow and weak bands corresponding to Tm-centred f–f excitation are also observed. Overall, these observations suggest that the ligand's sensitization of this ion is not as good as in previous compounds.

To further analyse the emissive properties, the decay curves were recorded at the most intense emission wavelengths to check the lifetimes of the corresponding excited states: 606 nm ($^4G_{5/2}$) for $\mathbf{2_{Sm}}$, 578 nm ($^4F_{9/2}$) for $\mathbf{3_{Dy}}$ and 482 nm ($^1G_4$) for $\mathbf{5_{Tm}}$. Accordingly, the curves were fitted to a multi-exponential expression ($I_t = A_0 + A_1 \exp(t/\tau_1) + A_2 \exp(t/\tau_2)$), note that only a second emissive component needed to be included in the fitting for $\mathbf{3_{Dy}}$, probably derived from a negligible contribution of the lamp's pulse in view of its low weight (see Fig. S21†). The lifetimes were estimated by means of the weighted sum of the components, obtaining the values of 43.3(1) μs (for $\mathbf{2_{Sm}}$, see Fig. S18†) and 18.7(6) μs (for $\mathbf{3_{Dy}}$, Fig. S21†). In the case of $\mathbf{5_{Tm}}$, the lifetime could not be estimated due to the weakness of the emitted signal. These results are in line with other previously reported CPs based on similar oxygen-donor based Ln centres.[54,55]

Cooling of the samples to 15 K, the emission patterns of the compounds experience some subtle differences, with the samples of $\mathbf{2_{Sm}}$ and $\mathbf{5_{Tm}}$ showing the most remarkable changes. On the one hand, $\mathbf{2_{Sm}}$ presents a progressive increase of the Sm(III)-centred characteristic emission bands with respect to the ligand-centred band, which remains almost stable with the drop of the temperature. On the other hand, $\mathbf{5_{Tm}}$ reveals an opposite behaviour with the weak band at λ_{em} = 482 nm (assigned to the $^3H_6 \leftarrow {}^1G_4$ transition at the

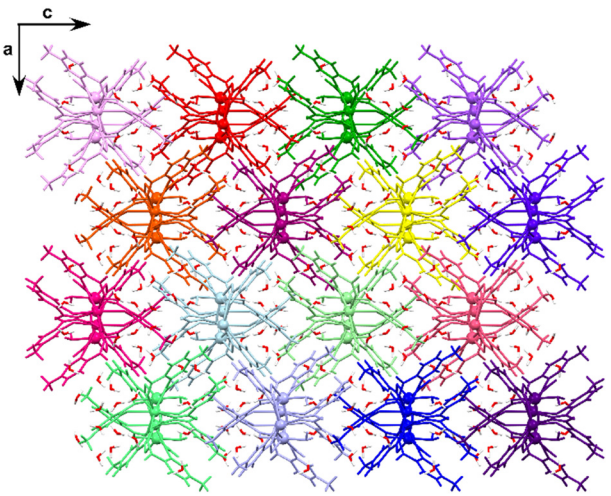

Fig. 2 View of the hydrogen bonded packing of compound $\mathbf{1_{Nd}}$ with 1D arrays highlighted in different colours. Crystallization water molecules are coloured using their habitual (previously mentioned) code.

Table 2 Photophysical properties of compounds $\mathbf{2_{Sm}}$, $\mathbf{3_{Dy}}$ and $\mathbf{5_{Tm}}$[a]

Comp.	λ_{ex}	λ_{em}	τ_{obs} 293 K	τ_{obs} 10 K	QY (%)
$\mathbf{2_{Sm}}$	370	390	0.3 ns	0.2 ns	2.8
	325	606	43.3 μs	39.0 μs	
$\mathbf{3_{Dy}}$	370	400	—	0.45 ns	6.2
	350	578	18.8 μs	28.2 μs	
$\mathbf{5_{Tm}}$	340	397	—	0.71 ns	1.6
	367	482	—	23.2 μs	

[a] Note that excitation wavelengths employed to analyze the lifetimes correspond to those fixed by the laser and led pulsed sources.

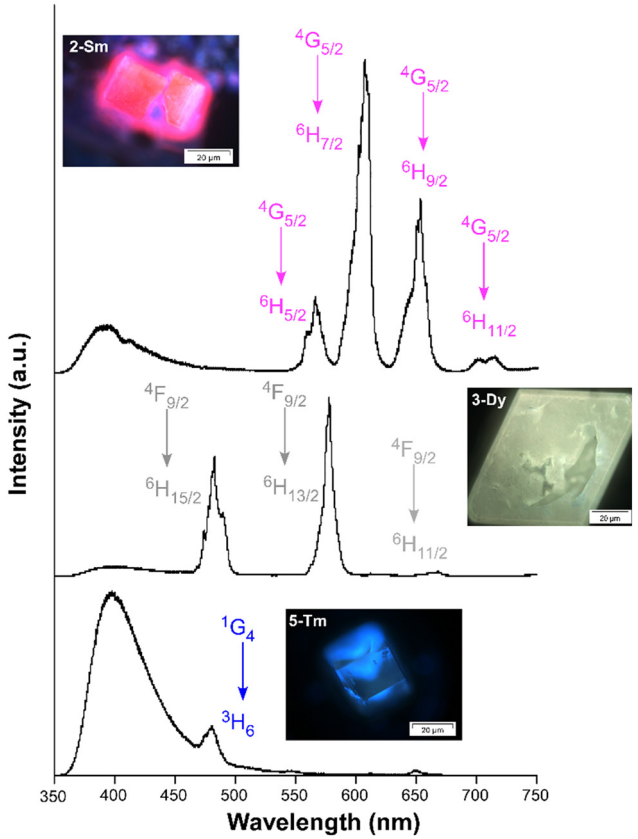

Fig. 3 Room temperature emission spectra of compounds $\mathbf{2_{Sm}}$, $\mathbf{3_{Dy}}$ and $\mathbf{5_{Tm}}$ together with the intraionic assignations. Micro-PL photographs of the emission of the samples (single crystals) under UV (λ_{ex} = 365 nm) light taken using a microscope.

Tm(III) centre), showing a very slight increase with the lowering of temperature in contrast to the strong increase occurring for the ligand-centred band. These relative evolutions occurring for the two types of bands in both samples give the opportunity of further inspecting the thermometric data according to a ratiometric analysis, in which the emission bands' intensity is integrated to avoid mistakes derived from analytical treatment. As observed in the plots shown in Fig. S25,† the relative emission (in terms of integrated ligand-centred *vs.* Ln-centred emissions) describes a linear curve for both compounds with the temperature, particularly showing a negative slope with the rising temperature. The best fitting results for the whole temperature range give the following equations for the self-referencing thermometric parameters (Δ_{Sm} = Int. I_{606}/Int. I_{390} and Δ_{Tm} = Int. I_{482}/Int. I_{397}):

$$\Delta_{Sm} = 1.0494–0.0044963T \text{ and } \Delta_{Tm} = 0.055062–0.000238T$$

with the maximum relative sensitivity (S_m) being 0.54 (at 225 K) and 0.35% K^{-1} (at 240 K) for compounds $\mathbf{2_{Sm}}$ and $\mathbf{5_{Tm}}$, respectively. Although it is true that these values are quite low compared to the best luminescent thermometers described so far (with S_m in the range of 7.1–16.0% K^{-1}),[50] those are based on Eu(III) and/or Tb(III) lanthanides and their co-doped mixtures. In contrast, it must be highlighted that these results are among the few reported thermometers based on Sm and Tm emitters, so their poorer thermometric activity could be compensated by other potential properties shown by these Lns. With regard to the lifetimes, those of $\mathbf{2_{Sm}}$ and $\mathbf{3_{Dy}}$ are not strongly affected, since they are kept to be 39.0(1) μs for $\mathbf{2_{Sm}}$ and 28.1(2) μs for $\mathbf{3_{Dy}}$. Conversely, a suitable decay curve of $\mathbf{5_{Tm}}$ could be measured at 10 K owing to the signal increase compared to RT, from which a lifetime of 23.21(2) μs was obtained (see Fig. S23†). Additionally, the absolute emission quantum yields (QYs) were also measured in the solid state at room temperature by means of an integrating sphere, using the same excitation wavelengths. Among them, compound $\mathbf{3_{Dy}}$ showed the highest QY with a value of 6.2%, followed by $\mathbf{2_{Sm}}$ with 2.8% and a low value of 1.6% for $\mathbf{5_{Tm}}$. The trend of the QY may be related to the energy transfer efficiency between the donor triplet state and the receptor Ln-based excited state, which is also connected to their relative energy gap. Taking into account that the triplet state responsible for the phosphorescent emission is estimated to lie at *ca.* 22 900 cm^{-1} over the ground state (estimated on the basis of the zero-phonon line for an isostructural Gd-based counterpart, see Fig. S30†) and that the emitting states of Ln ions are known to lie at the following energies: $^4F_{9/2}$ for Dy(III) ≈ 20 800 cm^{-1},[48] $^4G_{5/2}$ for Sm(III) ≈ 17 700 cm^{-1},[56] and $^1G_4$ for Tm(III) ≈ 21 500 cm^{-1},[57] it may be stated that the system obeys Latva's empirical rule.[58] This rule predicts that the optimal ligand-to-metal energy transfer process occurs when the aforementioned energy gap falls in the 2500–4000 cm^{-1} range, and this would explain why the dysprosium-based compound (with a T_1-$^4F_{9/2}$ gap of 2100 cm^{-1}) has the highest QY among the studied compounds. In fact, the triplet-$^1G_4$ energy gap for $\mathbf{5_{Tm}}$ seems to be too small (of *ca.* 1400 cm^{-1}) to favour the energy transfer, in line with the prediction raised by Latva that establishes a minimum energy gap of 1850 cm^{-1} between the triplet and the Ln-based intraionic donor state to avoid the back-transfer to the triplet manifold.[58]

PL properties of the Dy-based aqueous complex

In order to analyse the luminescence properties of the compounds dissolved in water, we have chosen the dysprosium-based compound as it is the most interesting because it resembles white light. This coordination polymer, $\mathbf{3_{Dy}@H_2O}$, characterized by a salty crystal structure in which $[Dy(\mu\text{-}6m2onic)_4]^-$ anionic complexes are joined together by $[Na(H_2O)^3]^+$ cationic fragments into 1D arrays, is quite soluble in water (*ca.* 14.5 mg mL^{-1}). In order to corroborate the stability of the complex in water (this solvent was selected due to its "green" character, biocompatibility and large applicability), ESI-MS (electrospray ionization-mass spectrometry) was used to characterize the speciation of the dissolved species in solution. As shown in Fig. S31,† the ESI^- MS spectrum presents a very intense signal centred at an *m*/*z*

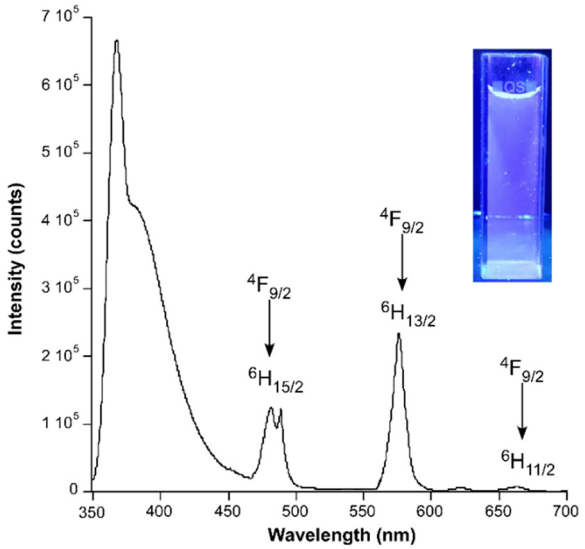

Fig. 4 Emission spectrum of $\mathbf{3_{Dy}@H_2O}$ under ligand band excitation wavelength. The inset shows its actual PL under a UV lamp with λ_{ex} = 365 nm.

of 771 which possesses a periodicity of one unit, thus confirming the presence of the $[Dy(\mu\text{-}6m2onic)_4]^-$ complex as the majority species in the solution. Moreover, photophysical measurements were also conducted. First, the UV-vis spectrum of a $\mathbf{3_{Dy}@H_2O}$ solution in a concentration of 1.25 mg mL^{-1} (used as a reference) presents a similar pattern to that of the solid state, with a remarkable hypsochromic shift of 30 nm for the former spectrum. Moreover, the integrity of the complex in solution can be further corroborated by the slight shift of the absorption bands existing between the complex and the free ligand (Fig. S15†).

The PL spectra and QY measurement of the aqueous solution show similar characteristics to those of the solid state. However, there are some important differences (Fig. 4): i) the excitation spectrum does not significantly change with respect to that of the solid state but for a proportional blue-shift to that observed in the absorption spectra; ii) ligand-centred emission dominates the spectrum against the characteristic f–f bands, which promotes a shift of the overall emission colour to bright blue (0.32, 0.30 coordinates in CIE1931). The lifetime of the characteristic intraionic transitions is almost the same (11.19 *vs.* 18.78 μs respectively for $\mathbf{3_{Dy}@H_2O}$ and $\mathbf{3_{Dy}}$), as it also happens for the ligand-centred fluorescence signal (0.384 *vs.* 0.454 ns respectively for $\mathbf{3_{Dy}@H_2O}$ and $\mathbf{3_{Dy}}$). As can be seen in the photograph taken on the UV illuminated aqueous solution, the compound shows blue-white emission which agrees with the emission spectrum dominated by the ligand's fluorescence. The QY of this aqueous complex was also explored and it can be said that the efficiency of the compound is almost maintained in aqueous solution (5.5 *vs.* 6.2% respectively for $\mathbf{3_{Dy}@H_2O}$ and $\mathbf{3_{Dy}}$). To finish this section, we also explored the effect of the complex concentration in the solution, for which the photoluminescence properties of three solutions with concentrations ranging from 0.75 to 3 mg mL^{-1} were analysed. As observed in Fig. S34,† both the main ligand-centred excitation band and the Dy-centred characteristic bands experience a progressive increase in intensity as the concentration of the complex increases from 0.75 to 1.75 mg mL^{-1}, although the relative increase is higher for the Dy-centred bands. At higher concentrations, the signal seems to be almost maintained, in fact the emission patterns recorded for $\mathbf{3_{Dy}@H_2O}$ at concentrations of 1.75 and 2.5 mg mL^{-1} are overlapped, meaning that 1.75 mg mL^{-1} could be an optimal concentration of the complex in terms of emission capacity. This effect can be better observed by comparing the relative emission of the Dy- (λ_{em} = 576 nm) and ligand-centred bands in terms of the integrated signal (Fig. S35†), where the Dy/ligand emission ratio rises abruptly from 0.75 to 1.75 mg mL^{-1} but reaches a plateau for higher concentrations. A similar trend is observed for the emission lifetimes (Fig. S36–S38†), showing decreasing and increasing trends respectively for the ligand- and Dy-centred bands, in such a way that lifetimes remain at *ca.* 1 ns and 12 μs. These effects confirm the increase of the ligand-to-metal transfer efficiency. The measurements of the QYs for these samples are also in line with previous results by showing a slight increase (from 5.5 up to 5.9%) for $\mathbf{3_{Dy}@H_2O}$ solutions at concentrations ≥ 1.75 mg mL^{-1}.

PL properties of lanthanide ion mixtures to yield white light emitters

Based on the excellent luminescence properties of this family of compounds, characterized by intense and stable long-lasting emission, we decided to prepare a series of heterometallic compounds by doping variable proportions of ions in order to modulate the emission colour, particularly with the aim of tuning white light in view of its enormous

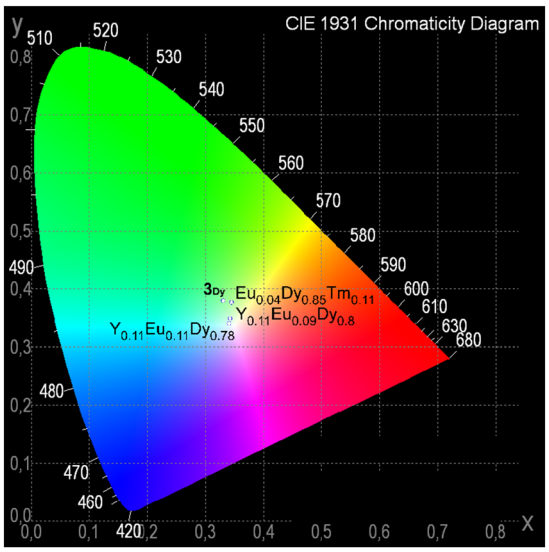

Fig. 5 CIE chromaticity diagram where the doped compounds appear.

technological interest, as previously pointed out, in the market of luminous devices.[36] To this end, compound $\mathbf{3_{Dy}}$ was taken as a base taking advantage of the fact that its emission is quite close to white light (with CIE (0.33, 0.37) coordinates, Fig. 5) as a result of the blue and orange contributions associated with its $^6H_{15/2} \leftarrow {}^4F_{9/2}$ and $^6H_{13/2} \leftarrow {}^4F_{9/2}$ transitions, respectively. Then, given the dominating net green emission of the compound, small amounts of Eu(III) were introduced into this compound to replace some of the Dy(III) in order to shift the emission colour towards red and a third element to enhance the blue coloured emission in the material. In a first approach, we took advantage of the blue-emitting capacity of the Tm(III) ion to combine it with the mentioned ions, in such a way that the $Eu_{0.04}Dy_{0.85}Tm_{0.11}$ mixture was employed to prepare the heterometallic compound (note that the real composition, close to the intended one, was corroborated by X-ray fluorescence, see Table S3†). It must be noticed that the small proportion of Eu(III) obeys the fact that this ion was greatly sensitized by the ligand probably owing to the optimal gap existing between the triplet and the Ln excited states (with a T_1-$^5D_0$ gap of 2500 cm^{-1}). As observed in the emission spectrum (Fig. S39a†), such a small amount of Eu(III) in the sample is enough to show a sizeable band at 612 nm (attributed to the most intense signal of the ion corresponding to the $^7F_2 \leftarrow {}^5D_0$ transition), whereas the doubled proportion of the Tm(III) ion in the compound does not significantly affect the emission, being unable to increase the intensity of the band sited at *ca.* 480 nm (one must remember that the bands derived from the $^6H_{15/2} \leftarrow {}^4F_{9/2}$ and $^3H_6 \leftarrow {}^1G_4$ transitions of Dy(III) and Tm(III), respectively, are completely overlapped). A possible reason for this behaviour could be the existence of an intramolecular transfer between the excited states of these ions, *i.e.* Tm($^1G_4$) → Dy($^4F_{9/2}$), given the energy level.

In spite of the fact that the emitted colour was shifted to red, the lack of blue-emission enhancement does not significantly reduce the excess of green light. Moreover, the QY was kept almost equal with a slight increase to 6.7%. With the aim of boosting the blue colored emission of the heterometallic compounds, we resorted to the possibility of improving the ligand-centered fluorescence (a band centered at *ca.* 390 nm and thus providing bright blue emission) by using a metal ion lacking inherent emission, as is the case of the Y(III) ion characterized for its closed shell electronic configuration that disables intraionic transitions. It must be noted that the isostructural nature of the Y-6m2onic compound was first confirmed by PXRD data (Fig. S10†), and that the crystal structure of a multi-metal dysprosium(III)/europium(III)/yttrium(III) CP (named as $\mathbf{7_{DyEuY}}$) could be also determined. A first preparation with this second strategy was approached by keeping the same proportion of the blue luminophore (11% of Y in the present case) and slightly increasing the weight of Eu(III) to reduce the proportion of Dy(III) in the solid solution (in view of the excess of green luminophore in the compound), in such a way that the $Dy_{0.8}Eu_{0.09}Y_{0.11}$ mixture was obtained. As observed in the corresponding emission spectrum (Fig. S39b†), the green signal (λ_{em} = 565 nm of the $^6H_J \leftarrow {}^4F_{9/2}$ transition) loses intensity with respect to the blue (ligand's fluorescence) and red (λ_{em} = 612 nm corresponding to the $^7F_2 \leftarrow {}^5D_0$ transition of Eu(III)) chromophores, which is translated in a shift of the resulting emitted colour (convoluted to the CIE pattern) in the appropriate direction. Finally, in a second attempt to get closer to the white light, the mixture of luminophores was fixed to the $Dy_{0.77}Eu_{0.12}Y_{0.11}$ ratio, which allowed somehow the intensity of the bands to be equalized and white light to be rendered with high purity ((0.34, 0.34) coordinates in the CIE1931 colour diagram). In addition to improving the quality of white emission with regard to the compound $\mathbf{3_{Dy}}$, the QY value was also greatly increased up to 15.8% (almost tripling the value of $\mathbf{3_{Dy}}$), which can be considered as a promising value and qualifies this material among the medium top results reported for white light emitters.[37] In particular, though a conscious analysis of the quantum efficiency of white-light emitters is limited because these data are scarcely reported, the quantum efficiency of herein described $\{[Dy_{0.77}Eu_{0.12}Y_{0.11}(6m2onic)_4Na(H_2O)_3]\cdot 8H_2O\}_n$ compound is classified above the half of most efficient (highest QY) white-light emitters based on Ln-CPs (see Table S4†). Moreover, and more importantly, we can confirm that the present compound, as far as we are aware, holds at the top of the particular classification of Dy-based heterometallic CPs showing white-light emission in terms of quantum efficiency.

PL properties of NIR emitters ($\mathbf{1_{Nd}}$, $\mathbf{4_{Er}}$ and $\mathbf{6_{Yb}}$)

Finally, the potential emission capacity of compounds $\mathbf{1_{Nd}}$, $\mathbf{4_{Er}}$ and $\mathbf{6_{Yb}}$ in the NIR range was also checked. At room temperature, the photoluminescence characterization of compounds revealed that, under UV laser light (λ_{ex} = 325 nm), they exhibit a wide band in which the maxima are centred at 387, 396 and 393 nm, respectively (see Fig. S41, S44 and S46†). As corroborated by the decay curves measured for these emission maxima, the emitted signal is composed of a very short fluorescence (of below 1 ns), meaning that the bands are assigned to the ligand fluorescence (see Fig. S43, S45 and S48†). In this sense, the narrow shape of the bands together with the absence of phosphorescent emission, as also observed for $\mathbf{2_{Sm}}$, $\mathbf{3_{Dy}}$ and $\mathbf{5_{Tm}}$, suggests that, assuming that low-lying triplet states will be populated in view of their isostructural nature, these compounds could present good energy transfers to these Lns and show Ln-centred emissions. Under these conditions, compound $\mathbf{4_{Er}}$ also presents a clear emission in the NIR region that is characteristic for the Er(III) ion, being majorly composed of a weak band peaking at 1537 nm corresponding to the $^4I_{15/2} \leftarrow {}^4I_{13/2}$ transition (Fig. S44†). Most of the CPs show no NIR emission at room temperature because these transitions are easily quenched by their coupling with molecular vibrations, meaning that this result can be considered as a consequence of the good encapsulation of Ln ions by the four-chelating

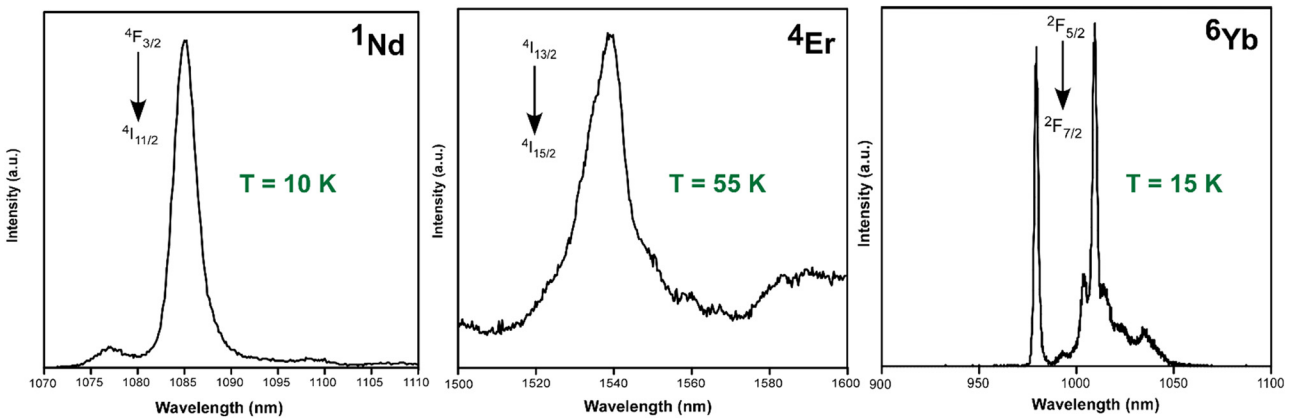

Fig. 6 Emission spectra of compounds $\mathbf{1_{Nd}}$, $\mathbf{4_{Er}}$ and $\mathbf{6_{Yb}}$ under UV excitation monitoring the ligand-centred band (λ_{ex} = 325 nm).

chromophore.[59] The change of the emission at low temperature was also studied for the samples with the aim of boosting the NIR emission. As observed in Fig. 6, the three compounds present narrow emission multiplets spanning in the 1075–1100, 1520–1600 and 975–1050 nm ranges corresponding to their characteristic $^4F_{3/2} \leftarrow {}^4F_{11/2}$, $^4I_{15/2} \leftarrow {}^4I_{13/2}$ and $^2F_{7/2} \leftarrow {}^2F_{5/2}$ transitions, respectively.

Among these signals, it is particularly worth mentioning that shown by $\mathbf{6_{Yb}}$, consisting of a sharp band peaking at 979 nm and a well-resolved multiplet with the most intense signal peaking at 1009 nm, which is a consequence of the significant crystal field generated by the four-chelating octacoordinated environment displayed by the 6m2onic ligands. The fitting of the decay curves for the three compounds at their main emission lines gives lifetimes of 305, 740 and 5127 ns, respectively for $\mathbf{1_{Nd}}$, $\mathbf{4_{Er}}$ and $\mathbf{6_{Yb}}$. The measured values fall in the range of previously reported Nd/Er/Yb-based complexes.[59–61]

Conclusions

The synthesis, physicochemical and structural characterization and PL performance of six isostructural heterometallic coordination polymers formed from distinct Ln and sodium ions and 6m2onic ligands, as well as of a multi-metal dysprosium(III)/europium(III)/yttrium(III) compound, are herein described in detail. These compounds with a $\{[Ln(6m2onic)_4Na(H_2O)_3]\cdot 8H_2O\}_n$ formula consist of 1D arrays of Ln and Na ions sequentially interconnected through 6m2onic ligands, with the four-chelating octacoordinated square antiprismatic environments of Ln ions being the most remarkable feature. Their crystal structure is completed by an extensive hydrogen bonding network tailored by lattice water molecules that packs the chains to one another into a 3D architecture. The compounds, especially $\mathbf{2_{Sm}}$ and $\mathbf{3_{Dy}}$, present good emission capacity under UV irradiation in the solid state characterized by intense lanthanide-centred characteristic emissions and relatively weak ligand-centred bands in the near UV-blue region, which suggests that an adequate antenna effect takes place. The sensitization of these ions seems to be a consequence of the eight-coordinated chromophores established in the $[Ln(\mu\text{-}6m2onic)_4]^-$ anionic complexes, in which the carboxylate/ketone moieties of 6m2onic ligands can be viewed as β-diketones, isolating the Ln ions from each other and promoting large energy transfers. This environment is also able to sensitize these Ln ions presenting NIR emission, rendering weak but sizeable emissions at 1537 nm for the Er(III) counterpart. Strong and narrow characteristic emission bands are also observed for Nd(III)-, Er(III)- and Yb(III)-based compounds at low temperature in the 1075–1100, 1520–1600 and 975–1050 nm ranges, respectively.

Taking advantage of the significant solubility of these compounds in water (*ca.* 14.5 mg mL^{-1}), probably derived from the salty nature of the crystal structure composed of $[Ln(\mu\text{-}6m2onic)_4]^-$ and $[Na(H_2O)_3]^+$ fragments, the photoluminescence characterization has been performed for $\mathbf{3_{Dy}}$ given its good emissive properties in the solid state. Once dissolved, anionic $[Dy(\mu\text{-}6m2onic)_4]^-$ complexes are stable in solution as confirmed by ESI-mass spectroscopy and present similar emission properties compared to the solid state, with the ligand-centred fluorescence signal now dominating the emission spectrum being the most remarkable difference. This enhancement, in addition to the decrease of the lifetime of the intraionic $^6H_{13/2} \leftarrow {}^4F_{9/2}$ transition, seems to indicate that the antenna effect is slightly worsened compared to the solid state. An analysis of photoluminescence properties at variable concentration reveals that 1.75 mg mL^{-1} is optimal to exploit the efficient emission of the aqueous complex.

Finally, the almost white light emitted by the Dy-based compound in the solid state (with (0.34, 0.38) coordinates in the CIE1931 pattern) gives the opportunity to fine-tune this emission colour to reach almost pure emitters by the doping strategy of metal ions. In particular, bright white emission with (0.34, 0.34) coordinates is achieved for the sample containing the $Dy_{0.77}Eu_{0.12}Y_{0.11}$ ratio for the crystallographic position of the Ln atom in the framework, as corroborated by the single crystal X-ray structure, in which the emission quantum yield is in turn increased up to 15.8%, which, as far as we are aware, holds at the top of Dy-based heterometallic

CPs showing white-light emission in terms of quantum efficiency.

Experimental section

Synthesis of $\{[Ln(6m2onic)_4Na(OH_2)_3]\cdot 8H_2O\}_n$ [where Ln(III) = Nd ($\mathbf{1_{Nd}}$), Sm ($\mathbf{2_{Sm}}$), Dy ($\mathbf{3_{Dy}}$), Er ($\mathbf{4_{Er}}$), Tm ($\mathbf{5_{Tm}}$), Yb ($\mathbf{6_{Yb}}$) and $Dy_{0.77}Eu_{0.12}Y_{0.11}$ ($\mathbf{7_{DyEuY}}$)]

All compounds were obtained by slowly dropping an aqueous solution of the corresponding lanthanide(III) nitrate hydrated salt (0.1 mmol, using 0.0438 g for $Nd(NO_3)_3\cdot 6H_2O$, 0.0444 g for $Sm(NO_3)_3\cdot 6H_2O$, 0.0438 g for $Dy(NO_3)_3\cdot 5H_2O$, 0.0443 g for $Er(NO_3)_3\cdot 5H_2O$, 0.0355 g for $Tm(NO_3)_3\cdot 6H_2O$ and 0.0453 g for $Yb(NO_3)_3\cdot 6H_2O$) over an aqueous-methanolic solution (4 mL, 1 : 1) of 6m2onic (0.4 mmol, 0.0613 g). Under continuous stirring, 3 mL of a 1 M NaOH aqueous solution was added dropwise, after which the solutions were poured into glass vials and allowed to slowly evaporate at room temperature. Well-shaped single crystals were grown after 3 days, which were filtered and washed with MeOH. Yield (based on metal): 45–55%. Anal. calcd. for $C_{28}H_{46}NdN_4NaO_{23}$ ($\mathbf{1_{Nd}}$) (%): C, 34.53; H, 4.76; N, 5.75. Found: C, 34.65; H, 4.62; N, 5.81. Anal. calcd. for $C_{28}H_{46}SmN_4NaO_{23}$ ($\mathbf{2_{Sm}}$) (%): C, 34.32; H, 4.73; N, 5.72. Found: C, 34.61; H, 4.52; N, 5.79. Anal. calcd. for $C_{28}H_{46}DyN_4NaO_{23}$ ($\mathbf{3_{Dy}}$) (%): C, 33.90; H, 4.67; N, 5.65. Found: C, 34.15; H, 4.45; N, 5.83. Anal. calcd. for $C_{28}H_{46}ErN_4NaO_{23}$ ($\mathbf{4_{Er}}$) (%): C, 33.73; H, 4.65; N, 5.62. Found: C, 33.80; H, 4.51; N, 5.77. Anal. calcd. for $C_{28}H_{46}TmN_4NaO_{23}$ ($\mathbf{5_{Tm}}$) (%): C, 33.69; H, 4.64; N, 5.61. Found: C, 33.79; H, 4.55; N, 5.74. Anal. calcd. for $C_{28}H_{46}YbN_4NaO_{23}$ ($\mathbf{6_{Yb}}$) (%): C, 33.54; H, 4.62; N, 5.59. Found: C, 33.61; H, 4.45; N, 5.67.

Finally, the multi-metal CP was synthesized with the same procedure but using the corresponding proportions for the lanthanide(III) nitrates, which were weighed in the starting metal solution. The real metal content mixture in the resulting crystals was estimated by means of X-ray fluorescence analysis, and that content was fixed in the crystal structure determination.

Chemical measurements

Elemental analyses (C, H, N) were performed on a Leco CHNS-932 microanalyzer. IR spectra were acquired with diluted KBr pellets using a ThermoNicolet IR 200 spectrometer in the 4000–400 cm^{-1} spectral region. Thermal analyses (TG/DTA) were performed on a TA Instruments SDT 2960 thermal analyzer in a synthetic air atmosphere (79% N_2/21% O_2) with a heating rate of 5 °C min^{-1}. X-ray fluorescence measurements on the doped samples were carried out on a wavelength dispersed X-ray fluorescence (XRF) sequential spectrometer (PANalytical AXIOS) to determine the amounts of Y/Ln ions present in the samples. Diffuse reflectance and UV-vis measurements were recorded at room temperature on a UV-2600 UV/vis Shimadzu spectrophotometer using polycrystalline samples of all compounds and $\mathbf{3_{Dy}@H_2O}$ solution, employing $BaSO_4$ and distilled water as references, respectively, for solid and liquid samples.

X-ray diffraction data collection and structure determination

X-ray data collection was done on suitable single crystals of compounds $\mathbf{1_{Nd}}$ and $\mathbf{5_{Tm}}$ and the multi-metal $\mathbf{7_{DyEuY}}$ on a Bruker VENTURE diffractometer equipped with an area detector and graphite monochromated Mo K_α radiation (λ = 0.71073 Å) through the ω-scan method at 130(2) K. The data reduction was performed with the APEX2[62] software, correcting the absorption of the crystal with SADABS.[63] The crystal structures were solved by direct methods using the SHELXT program[64] and refined by full-matrix least-squares on F^2 including all reflections with the OLEX2 crystallographic package.[65] All hydrogen atoms were introduced in the difference Fourier map as fixed contributions using riding models with isotropic thermal displacement parameters of 1.2 (for the aromatic C–H atoms of the pyridine ring of the ligand) or 1.5 times (for the methyl groups and water molecules) those of their linked heteroatoms. The Dy/Eu/Y ratio refined in the structure of compound $\mathbf{7_{DyEuY}}$ corresponds to the results obtained from the XRF technique (see Table S3†). The main crystallographic details and refinement data are gathered in Table 3. Crystallographic data have been deposited with the Cambridge Crystallographic Data Center (ESI†)with CCDC no. 2378019–2378021.

The X-ray powder diffraction (XRPD) patterns were measured on ground single crystals or polycrystalline samples with a Philips X'PERT powder diffractometer equipped with Cu-Kα radiation (λ = 1.5418 Å). The patterns were acquired over the $5 < 2\theta < 50°$ range with a step size of 0.026° and an acquisition time of 2.5 s per step at 25 °C. Indexation of the diffraction profiles was made using the FULLPROF program (pattern matching analysis)[66] on the basis of the space group and cell parameters obtained for single crystal X-ray diffraction.

Photoluminescence measurements

Fluorescence excitation and emission spectra and lifetime measurements in the solid state were recorded on an Edinburgh Instruments FLS920 spectrometer at variable temperature using a closed cycle helium cryostat enclosed in the spectrometer. All samples were first placed under high vacuum (of *ca.* 10^{-9} mbar) to avoid the presence of oxygen or water in the sample holder. For steady-state measurements, a Müller-Elektronik-Optik SVX1450 Xe lamp or an IK3552R-G He–Cd continuous laser (325 nm) was used as an excitation source, whereas a microsecond pulsed μF900 lamp coupled to the spectrometer was used for the long-lived (lifetimes of few milliseconds) emissions and a PLS-340 pulsed led of PicoQuant (λ = 340 nm) or an LDH-FA-370 pulsed laser of PicoQuant (λ = 370 nm) was used for the short-lived (of nanoseconds) emissions. The emission spectra in the NIR region and the decay curves were acquired on a Hamamatsu NIR-PMT H10330C-75 detector, setting the detector voltage at 800 V. The quantum yield was measured in the solid state by means of a Horiba Quanta-f integrating sphere using an Oriel

Table 3 Single crystal X-ray diffraction data and structure refinement details of compounds $\mathbf{1_{Nd}}$, $\mathbf{5_{Tm}}$ and $\mathbf{7_{DyEuY}}$

Compound	$\mathbf{1_{Nd}}$	$\mathbf{5_{Tm}}$	$\mathbf{7_{DyEuY}}$
Empirical formula	$C_{28}H_{46}NdN_4NaO_{23}$	$C_{28}H_{46}TmN_4NaO_{23}$	$C_{28}H_{46}Dy_{0.77}Eu_{0.12}Y_{0.10}N_4NaO_{23}$
Formula weight	973.92	998.61	981.81
Crystal system	Orthorhombic	Orthorhombic	Orthorhombic
Space group	*Pbca*	*Pbca*	*Pbca*
a (Å)	18.2627(7)	18.7780(6)	22.937(5)
b (Å)	18.6667(9)	22.8484(6)	18.160(4)
c (Å)	22.9380(9)	18.0407(6)	18.791(4)
V (Å^3)	7819.7(6)	7740.3(4)	7827(3)
Reflections collected	84 592	64 038	96 067
Unique data/parameters	11 939/551	8284/518	8018/530
R_{int}	0.0391	0.0548	0.0562
GoF (S)[a]	1.033	1.050	1.125
R_1[b]/wR_2[c] [$I > 2\sigma(I)$]	0.0245/0.0603	0.0268/0.0493	0.0445/0.0838
R_1[b]/wR_2[c] [all]	0.0324/0.0645	0.0479/0.0583	0.0753/0.1118

[a] $S = [\sum w(F_0^2 - F_c^2)^2/(N_{obs} - N_{param})]^{1/2}$. [b] $R_1 = \sum||F_0| - |F_c||/\sum|F_0|$. [c] $wR_2 = [\sum w(F_0^2 - F_c^2)^2/\sum wF_0^2]^{1/2}$; $w = 1/[\sigma^2(F_0^2) + (aP)^2 + bP]$ where $P = (\max(F_0^2, 0) + 2Fc^2)/3$ with $a = 0.0284$ and $b = 5.8623$ ($\mathbf{1_{Nd}}$); $a = 0.0140$ and $b = 11.2497$ ($\mathbf{5_{Tm}}$) and $a = 0.0001$ and $b = 84.3999$ ($\mathbf{7_{DyEuY}}$).

Instruments MS257 lamp as the excitation source and an iHR550 spectrometer from Horiba to analyse the emission. Five measurements were accomplished to properly estimate the mean and standard deviation values for each compound. Photographs of irradiated single-crystals and polycrystalline samples were taken at room temperature in a micro-PL system included in an Olympus optical microscope illuminated with a Hg lamp.

Computational details

The Gaussian 16 package[67] was employed for the geometry optimizations and the TDDFT calculations on the appropriate models of compound $\mathbf{3_{Gd}}$. The calculations were performed at the B3LYP level of theory with the 6-311++G(d,p) basis set[68] for all atoms and the MWB50 pseudo-potential for Nd(III).[69]

Data availability

The data supporting this article have been included as part of the ESI† and will be available from the authors upon reasonable request. Moreover, the crystallographic data for $\mathbf{1_{Nd}}$, $\mathbf{5_{Tm}}$ and $\mathbf{7_{DyEuY}}$ have been deposited at the CCDC under 2378019–2378021.

Conflicts of interest

There are no conflicts to declare.

Acknowledgements

This work has been funded by Red Guipuzcoana de Ciencia, Tecnología e Innovación (FA385/2023, DG23/16), Gobierno Vasco/Eusko Jaurlaritza (IT1755-22 and IT1500-22), and Junta de Andalucía (FQM-394 and P21_00386). L. R. B. is grateful to the UPV/EHU for his predoctoral grant. The authors acknowledge technical and human support provided by SGIker (UPV/EHU/ERDF, EU).

References

1 S. R. Batten, B. Chen and J. J. Vittal, *ChemPlusChem*, 2016, **81**, 669–670.
2 D. Li, A. Yadav, H. Zhou, K. Roy, P. Thanasekaran and C. Lee, *Global Challenges*, 2024, **8**, 2300244.
3 L. Jiao, J. Y. R. Seow, W. S. Skinner, Z. U. Wang and H.-L. Jiang, *Mater. Today*, 2019, **27**, 43–68.
4 W. Lu, Z. Wei, Z. Y. Gu, T. F. Liu, J. Park, J. Park, J. Tian, M. Zhang, Q. Zhang, T. Gentle, M. Bosch and H. C. Zhou, *Chem. Soc. Rev.*, 2014, **43**, 5561–5593.
5 V. Guillerm, D. Kim, J. F. Eubank, R. Luebke, X. Liu, K. Adil, M. S. Lah and M. Eddaoudi, *Chem. Soc. Rev.*, 2014, **43**, 6141–6172.
6 J. M. Frost, K. L. M. Harriman and M. Murugesu, *Chem. Sci.*, 2016, **7**, 2470–2491.
7 J. Heine and K. Müller-Buschbaum, *Chem. Soc. Rev.*, 2013, **42**, 9232–9242.
8 J.-C. C. G. Bünzli, *Coord. Chem. Rev.*, 2015, **293–294**, 19–47.
9 S. Shaw and J. D. White, *Chem. Rev.*, 2019, **119**, 9381–9426.
10 Y. C. Ong, S. Roy, P. C. Andrews and G. Gasser, *Chem. Rev.*, 2019, **119**, 730–796.
11 V. Stavila, A. A. Talin and M. D. Allendorf, *Chem. Soc. Rev.*, 2014, **43**, 5994–6010.
12 Z. Wang, H. Sezen, J. Liu, C. Yang, S. E. Roggenbuck, K. Peikert, M. Fröba, A. Mavrantonakis, B. Supronowicz, T. Heine, H. Gliemann and C. Wöll, *Microporous Mesoporous Mater.*, 2015, **207**, 53–60.
13 W. P. Lustig, S. Mukherjee, N. D. Rudd, A. V. Desai, J. Li and S. K. Ghosh, *Chem. Soc. Rev.*, 2017, **46**, 3242–3285.
14 P. Horcajada, R. Gref, T. Baati, P. K. Allan, G. Maurin, P. Couvreur, G. Férey, R. E. Morris and C. Serre, *Chem. Rev.*, 2012, **112**, 1232–1268.
15 L. Ma, C. Abney and W. Lin, *Chem. Soc. Rev.*, 2009, **38**, 1248–1256.
16 G. M. Espallargas and E. Coronado, *Chem. Soc. Rev.*, 2018, **47**, 533–557.

17 Y. Cui, B. Chen and G. Qian, *Coord. Chem. Rev.*, 2014, **273–274**, 76–86.
18 J. Rocha, L. D. Carlos, F. A. A. Paz and D. Ananias, *Chem. Soc. Rev.*, 2011, **40**, 926–940.
19 R. J. Kuppler, D. J. Timmons, Q. R. Fang, J. R. Li, T. A. Makal, M. D. Young, D. Yuan, D. Zhao, W. Zhuang and H. C. Zhou, *Coord. Chem. Rev.*, 2009, **253**, 3042–3066.
20 R. Layfield and M. Murugesu, *Lanthanides and Actinides in Molecular Magnetism*, Wiley, 2015.
21 D. Atwood, *The rare earth elements: fundamentals and applications*, 2013.
22 J.-C. G. Bünzli and C. Piguet, *Chem. Soc. Rev.*, 2005, **34**, 1048–1077.
23 S. Subudhi, D. Rath and K. M. Parida, *Catal. Sci. Technol.*, 2018, **8**, 679–696.
24 J. C. G. Bünzli, *Lanthanide Luminescence: From a Mystery to Rationalization, Understanding, and Applications*, Elsevier, 2016, vol. 50.
25 M. Hasegawa, H. Ohmagari, H. Tanaka and K. Machida, *J. Photochem. Photobiol., C*, 2022, **50**, 100484.
26 J. Andres and A. S. Chauvin, *Molecules*, 2020, **25**, 4022.
27 Y. Kitagawa, A. Naito, K. Fushimi and Y. Hasegawa, *RSC Adv.*, 2021, **11**, 6604–6606.
28 S. R. Zheng, J. B. Tan, S. L. Cai, J. Fan and W. G. Zhang, *CrystEngComm*, 2016, **18**, 8672–8682.
29 Z. G. Gu, H. C. Fang, P. Y. Yin, L. Tong, Y. Ying, S. J. Hu, W. S. Li and Y. P. Cai, *Cryst. Growth Des.*, 2011, **11**, 2220–2227.
30 J. Y. Gao, N. Wang, X. H. Xiong, C. J. Chen, W. P. Xie, X. R. Ran, Y. Long, S. T. Yue, Y. L. Liu and Y. P. Cai, *Inorg. Chem. Commun.*, 2013, **37**, 197–201.
31 D. S. Yu, X. H. Zeng, P. Wang, X. H. Cao, H. H. Li and Z. R. Chen, *J. Cluster Sci.*, 2014, **25**, 581–590.
32 S. Abednatanzi, P. G. Derakhshandeh, H. Depauw, F. X. Coudert, H. Vrielinck, P. Van Der Voort and K. Leus, *Chem. Soc. Rev.*, 2019, **48**, 2535–2565.
33 J. X. Ma, T. Ma, R. Qian, L. Zhou, Q. Guo, J. H. Yang and Q. Yang, *Inorg. Chem.*, 2021, **60**, 7937–7951.
34 V. V. Utochnikova, A. Y. Grishko, D. S. Koshelev, A. A. Averin, L. S. Lepnev and N. P. Kuzmina, *Opt. Mater.*, 2017, **74**, 201–208.
35 B. Xu, D. Li, Z. Huang, C. Tang, W. Mo and Y. Ma, *Dalton Trans.*, 2018, **47**, 7534–7540.
36 B. Shao, J. Huo and H. You, *Adv. Opt. Mater.*, 2019, **7**, 1900319.
37 J. Wu, H. Zhang and S. Du, *J. Mater. Chem. C*, 2016, **4**, 3364–3374.
38 S. Petoud, S. M. Cohen, J. C. G. Bünzli and K. N. Raymond, *J. Am. Chem. Soc.*, 2003, **125**, 13324–13325.
39 G. L. Law, K. L. Wong, H. L. Tam, K. W. Cheah and W. T. Wong, *Inorg. Chem.*, 2009, **48**, 10492–10494.
40 G. L. Law, W. M. Kwok, W. T. Wong, K. L. Wong and P. A. Tanner, *J. Phys. Chem. B*, 2007, **111**, 10858–10861.
41 P. Martín-Ramos, C. Coya, Á. L. Álvarez, M. R. Silva, C. Zaldo, J. A. Paixão, P. Chamorro-Posada and J. Martín-Gil, *J. Phys. Chem. C*, 2013, **117**, 10020–10030.
42 J. D. B. Bradley and M. Pollnau, *Laser Photonics Rev.*, 2011, **5**, 368–403.
43 C. Wei, H. Wei, W. Yan, Z. Zhao, Z. Cai, B. Sun, Z. Meng, Z. Liu, Z. Bian and C. Huang, *Inorg. Chem.*, 2016, **55**, 10645–10653.
44 J. Wang, T. Lu, Y. Li, J. Wang and E. Spruijt, *Adv. Colloid Interface Sci.*, 2023, **318**, 102964.
45 L. Razquin-Bobillo, O. Pajuelo-Corral, A. Zabala-Lekuona, A. Rodríguez-Diéguez and J. Cepeda, *Dalton Trans.*, 2022, **51**, 16243–16255.
46 L. Razquin-Bobillo, O. Pajuelo-Corral, B. Artetxe, A. Zabala-Lekuona, D. Choquesillo-Lazarte, A. Rodríguez-Diéguez, E. San Sebastian, J. Cepeda, E. S. Sebastian and J. Cepeda, *Dalton Trans.*, 2022, **51**, 9780–9792.
47 S. Alvarez, D. Avnir, M. Llunell and M. Pinsky, *New J. Chem.*, 2002, **26**, 996–1009.
48 A. B. Ruiz-Muelle, A. García-García, A. García-Valdivia, I. Oyarzabal, J. Cepeda, J. M. Seco, E. Colacio, A. Rodríguez-Diéguez and I. Fernández, *Dalton Trans.*, 2018, **47**, 12783–12794.
49 Q. Yao, Y. Wang, B. Zhao, X. Zhu, Y. Luo, D. Yuan and Y. Yao, *Inorg. Chem.*, 2022, **61**, 10373–10382.
50 J. Rocha, C. D. S. Brites and L. D. Carlos, *Chem. – Eur. J.*, 2016, **22**, 14782–14795.
51 C. Y. Zhu, Z. Wang, J. T. Mo, Y. N. Fan and M. Pan, *J. Mater. Chem. C*, 2020, **8**, 9916–9922.
52 K. Binnemans, *Chem. Rev.*, 2009, **109**, 4283–4374.
53 A. Zabala-Lekuona, J. Cepeda, I. Oyarzabal, A. Rodríguez-Diéguez, J. A. García, J. M. Seco and E. Colacio, *CrystEngComm*, 2017, **19**, 256–264.
54 U. Huizi-Rayo, A. Zabala-Lekuona, A. Terenzi, C. M. C. M. Cruz, J. M. J. M. Cuerva, A. Rodríguez-Diéguez, J. A. J. A. García, J. M. J. M. Seco, E. San Sebastian and J. Cepeda, *J. Mater. Chem. C*, 2020, **8**, 8243–8256.
55 À. Tubau, L. Rodriguez, P. H. Pander, L. A. Weatherill, F. B. Dias, M. Font-Bardia and R. Vicente, *J. Mater. Chem. C*, 2024, **12**, 8127–8144.
56 H. Yamamoto, S. Shionoya and W. M. Yen, *Phosphor Handbook*, CRC Press, Taylor & Francis Group, 2nd edn, 2007.
57 T. Yu, H. Lin, D. Yu, S. Ye and Q. Zhang, *J. Phys. Chem. C*, 2015, **119**, 26643–26651.
58 M. Latva, H. Takalob, V. M. Mukkala, C. Matachescu, J. C. Rodríguez-Ubis and J. Kankare, *J. Lumin.*, 1997, **75**, 149–169.
59 A. Monguzzi, A. Milani, L. Lodi, M. I. Trioni, R. Tubino and C. Castiglioni, *New J. Chem.*, 2009, **33**, 1542–1548.
60 E. Cavalli, S. Ruggieri, S. Mizzoni, C. Nardon, M. Bettinelli and F. Piccinelli, *Results Chem.*, 2022, **4**, 100388.
61 E. Kasprzycka, A. N. Carneiro Neto, V. A. Trush, O. L. Malta, L. Jerzykiewicz, V. M. Amirkhanov, J. Legendziewicz and P. Gawryszewska, *Spectrochim. Acta, Part A*, 2022, **274**, 121072.
62 Bruker AXS Inc., Madison, 2004.
63 G. M. Sheldrick, *SADABS, Empirical Absorption Correction Program*, 1997.
64 G. M. Sheldrick, *Acta Crystallogr., Sect. A: Found. Adv.*, 2015, **71**, 3–8.

65 O. V. Dolomanov, L. J. Bourhis, R. J. Gildea, J. A. K. K. Howard and H. Puschmann, *J. Appl. Crystallogr.*, 2009, **42**, 339–341.
66 J. Rodríguez-Carvajal, *FULLPROF 2000, version 2.5d*, Lab. Léon Brillouin (CEA-CNRS), Cent. d'Études deSaclay, Gif sur Yvette Cedex, France, 2003.
67 M. J. Frisch, G. W. Trucks, H. B. Schlegel, G. E. Scuseria, M. A. Robb, J. R. Cheeseman, G. Scalmani, V. Barone, G. A. Petersson, H. Nakatsuji, X. Li, M. Caricato, A. V. Marenich, J. Bloino, B. G. Janesko, R. Gomperts, B. Mennucci, H. P. Hratchian, J. V. Ortiz, A. F. Izmaylov, J. L. Sonnenberg, D. Williams-Young, F. Ding, F. Lipparini, F. Egidi, J. Goings, B. Peng, A. Petrone, T. Henderson, D. Ranasinghe, V. G. Zakrzewski, J. Gao, N. Rega, G. Zheng, W. Liang, M. Hada, M. Ehara, K. Toyota, R. Fukuda, J. Hasegawa, M. Ishida, T. Nakajima, Y. Honda, O. Kitao, H. Nakai, T. Vreven, K. Throssell, J. A. J. Montgomery, J. E. Peralta, F. Ogliaro, M. J. Bearpark, J. J. Heyd, E. N. Brothers, K. N. Kudin, V. N. Staroverov, T. A. Keith, R. Kobayashi, J. Normand, K. Raghavachari, A. P. Rendell, J. C. Burant, S. S. Iyengar, J. Tomasi, M. Cossi, J. M. Millam, M. Klene, C. Adamo, R. Cammi, J. W. Ochterski, R. L. Martin, K. Morokuma, O. Farkas, J. B. Foresman and D. J. Fox, *Gaussian 16*, 2016.
68 V. A. Rassolov, J. A. Pople, M. A. Ratner and T. L. Windus, *J. Chem. Phys.*, 1998, **109**, 1223–1229.
69 M. Dolg, H. Stoll, A. Savin and H. Preuss, *Theor. Chim. Acta*, 1989, **75**, 173–194.